

Shock waves in a one-dimensional Bose gas: from a Bose-Einstein condensate to a Tonks gas

Bogdan Damski

Theory Division, Los Alamos National Laboratory, MS-B213, Los Alamos, NM 87545, USA

We derive and analyze shock-wave solutions of hydrodynamic equations describing repulsively interacting one dimensional Bose gas. We also use the number-conserving Bogolubov approach to verify accuracy of the Gross-Pitaevskii equation in shock wave problems. We show that quantum corrections to dynamics of shocks (dark-shock-originated solitons) in a Bose-Einstein condensate are negligible (important) for a realistic set of system parameters. We point out possible signatures of a Bose-Einstein condensate – Tonks crossover in shock dynamics. Our findings can be directly verified in different experimental setups.

PACS numbers: 03.75.Kk, 47.35.+i, 43.35.+d

I. INTRODUCTION

Physics of one dimensional (1D) Bose gases attracts more and more attention due to both very interesting phenomena that appear in these systems [1], and a very recent experimental progress toward realization of Tonks gases [2, 3, 4]. In this paper we provide a unified description of basic shock waves properties in 1D Bose gases interacting with arbitrary strength. Previous works on this subject were limited to either weakly interacting gases [5, 6, 7, 8, 9] or the strongly interacting ones [10]. We also describe influence of depleted atoms on dynamics of a Bose-Einstein condensate (BEC) shocks. Finally, we derive a simple expression for speed of propagation of arbitrarily shaped density pulses.

Sec. II describes theoretical basics of an approximate hydrodynamic approach. Sec. III discusses shock-wave solutions of this approach on specific examples. Sec. IV describes propagation of arbitrarily shaped pulses. Sec. V explains experimental methods used for generation of shock structures, while Sec. VI presents quantum corrections to shock solutions of the Gross-Pitaevskii equation. Finally, Sec. VII provides a summary of this paper.

II. THE MODEL

We consider delta interacting Bose gas in a 1D box. Its experimental realization is possible due to recent experimental progress in trapping of small samples of ultracold bosonic atoms in a box-like optical trap [4]. Another exciting experimental setup may come from a paper of Gupta *et al* [11], where successful realization of a ring shaped magnetic trap filled with a BEC was recently reported.

The Hamiltonian of our system in dimensionless quantities (see Appendix A for units) reads:

$$\hat{H} = -\frac{1}{2} \sum_{i=1}^N \frac{\partial^2}{\partial x_i^2} + a \sum_{i<j} \delta(x_i - x_j), \quad (1)$$

where $a > 0$ is the interaction coupling [12]. It turns out

that there is only one parameter that determines system static properties:

$$\gamma = \frac{a}{\rho}, \quad (2)$$

where ρ is atomic density normalized to $N \gg 1$. In the limit of $\gamma \rightarrow 0$ our system is a Bose-Einstein condensate, while when $\gamma \rightarrow +\infty$ it is a Tonks gas, whose properties are captured by the Fermi-Bose mapping theorem (FBMT) [13]. To see how big is a BEC-Tonks crossover one can look at sound velocity and compare it to BEC and Tonks predictions. Exact expression for sound velocity [14] (see also Appendix A) is

$$v_s = \rho \sqrt{3e(\gamma) - 2\gamma \frac{de}{d\gamma} + \frac{1}{2}\gamma^2 \frac{d^2e}{d\gamma^2}}, \quad (3)$$

where $e(\gamma)$ is defined by Lieb and Liniger in [15]. The v_s/ρ is depicted in Fig. 1 – notice how slowly the system enters a Tonks regime. A large BEC-Tonks crossover, $\gamma \sim (1, 50)$, provides us motivation for studies of shock waves outside BEC [5, 6, 7, 8, 9] and Tonks [10] limits.

Many-body solutions of (1) at zero absolute temperature have been analyzed in classic papers [14, 15]. These solutions are based on the Bethe ansatz and allow for analytical extraction of different static system properties. Unfortunately, they are too complicated for description of system dynamics.

To simplify the problem a proper hydrodynamical approach can be worked out [16, 17] and leads to the following set of equations

$$\frac{\partial \rho}{\partial t} + \frac{\partial}{\partial x} (v\rho) = 0, \quad (4)$$

$$\frac{\partial v}{\partial t} + \frac{\partial}{\partial x} \left(\frac{1}{2} v^2 \right) + \frac{\partial}{\partial x} \left(\mu(\rho) + V_l - \frac{1}{2} \frac{\partial_x^2 \sqrt{\rho}}{\sqrt{\rho}} \right) = 0 \quad (5)$$

where

$$\mu(\rho) = \frac{1}{2} \rho^2 \left(3e(\gamma) - \gamma \frac{de}{d\gamma} \right), \quad (6)$$

and V_l is an external potential acting on atoms. A nice property of these equations is that they exactly reproduce sound velocity (3), while the problems with their usage for description of shock propagation (not formation) come from their derivation valid in the long-wavelength limit, where the quantum pressure (QP) term,

$$\frac{1}{2} \frac{\partial_x^2 \sqrt{\rho}}{\sqrt{\rho}}, \quad (7)$$

is negligible.

To get more insight into physics described by (5) and validity of a QP term we look at BEC and Tonks limits. In the BEC case, $\mu(\rho) \rightarrow a\rho$ and Eqs. (4,5) can be obtained by time-dependent variational principle applied to a product wave function

$$\Psi(x_1, \dots, x_N, t) = \sqrt{N} \phi(x_1, t) \cdots \phi(x_N, t), \quad (8)$$

$\int dx |\phi(x, t)|^2 = 1$. It results in time-dependent Gross-Pitaevskii equation (29). Then substitution of $\phi = \sqrt{\rho} \exp(i\chi)$ and $v = \partial_x \chi$ into (29) gives a BEC version of (4,5). In other terms, ρ in (4,5) is a single particle density defined in a many-body theory as

$$\rho(x, t) = \int dx_2 \cdots dx_N |\Psi(x, x_2, \dots, x_N, t)|^2, \quad (9)$$

which equals $N|\phi(x, t)|^2$ in the BEC limit. A quantum pressure term in this limit is rigorously derived [18].

In the Tonks regime one has $\mu(\rho) \rightarrow \rho^2 \pi^2 / 2$, which was first found by renormalization group approach in [19, 20], and then used in a number of papers, e.g., [10, 21, 22]. Now derivation of (5), do not involve any sort of product simplification (8) of a wave-function. Indeed, a Fermi-Bose mapping theorem [13] implies, e.g., that if $\Psi_F(x_1, \dots, x_N)$ is a ground state wave-function of noninteracting fermions placed in the same potential as a Tonks gas, then a ground state Tonks wave-function is $|\Psi_F(x_1, \dots, x_N)|$. Therefore, even a simple description of a Tonks gas based on the single particle density (9) involves N orthogonal single particle orbitals instead of a single one, $\phi(x)$, used in the BEC case.

In Tonks limit the QP term was shown to lead to unphysical density oscillations [10, 23]. From knowledge that the quantum pressure term is present in the BEC limit $\gamma \rightarrow 0$ and absent in Tonks regime $\gamma \rightarrow +\infty$ it is clear that Eqs. (4,5) can not describe shock propagation for arbitrary γ . Nonetheless, shock formation from density perturbations that are initially wide can be successfully done, and will be described below. In this case the QP term is unimportant roughly up to shock formation. Due to lack of theoretical concepts for getting exact time-dependent solutions for the system of interest, we consider future experimental results as the best verification of our calculations based on hydrodynamic equations.

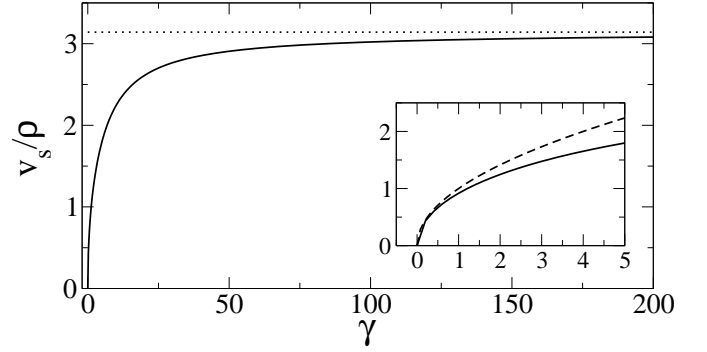


FIG. 1: Sound velocity divided by density. In the BEC limit ($\gamma \rightarrow 0$) it is $\sqrt{\gamma}$, while in the Tonks limit ($\gamma \rightarrow +\infty$) it equals π . Solid line: (3), dots: Tonks value, dashed line: $\sqrt{\gamma}$. For units see Appendix A.

III. SHOCK WAVE SOLUTIONS

The quantum pressure term (7) is important only when density changes occur on length scales smaller than the characteristic length given by

$$\xi(\rho) = \frac{1}{\sqrt{2\mu(\rho)}}. \quad (10)$$

In a BEC limit $\xi(\rho)$ is called a healing length, and we propose to use the same name regardless of γ .

Now we want to solve Eqs. (4,5,6). Assuming that the perturbation under consideration is, at least initially, broad compared to ξ , the quantum pressure term in (5) can be neglected. Following standard methods [24] one gets

$$\rho(x, t) = f \left(x - \left(\int d\rho \sqrt{\frac{1}{\rho} \frac{\partial \mu}{\partial \rho}} + \sqrt{\rho \frac{\partial \mu}{\partial \rho}} \right) t \right), \quad (11)$$

$$v(x, t) = \int d\rho \sqrt{\frac{1}{\rho} \frac{\partial \mu}{\partial \rho}}. \quad (12)$$

To proceed further with analytical calculations we use the following relations:

$$0 < \gamma < \gamma_c : \sqrt{\frac{1}{\rho} \frac{\partial \mu}{\partial \rho}} \approx \sqrt{\gamma} - \frac{\gamma}{4\pi} - \frac{\gamma^{3/2}}{32\pi^2} - \frac{\gamma^2}{128\pi^3}, \quad (13)$$

$$\gamma_c \leq \gamma : \sqrt{\frac{1}{\rho} \frac{\partial \mu}{\partial \rho}} \approx \frac{\pi}{(1 + 2/\gamma)^2}, \quad (14)$$

where $\gamma_c \approx 14.5$ from the requirement that both expansions match at γ_c . Expression (13) is extracted from Lieb's observation [14] that for $\gamma < \sim 10$

$$\sqrt{\frac{1}{\rho} \frac{\partial \mu}{\partial \rho}} \cong \sqrt{\gamma - \gamma^{3/2}/(2\pi)}. \quad (15)$$

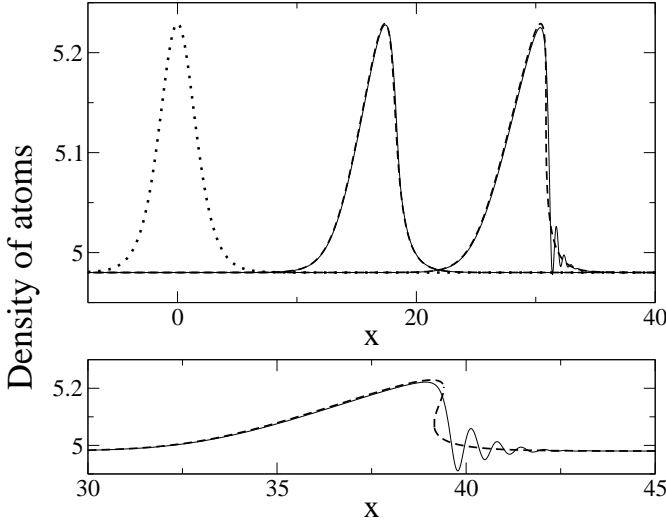


FIG. 2: Dotted line: initial density profile (16). Solid line: solution of Eqs. (4,5) with density at $t = 0$ given by (16) and velocity field determined from (12). Dashed line: implicit solution (18) multiplied by ρ_0 . Upper plot: subsequent density profiles correspond to $t = 0, 1.155, 2.02$. Lower plot: $t = 2.6$. Time of shock creation equals $t_s = 2.03$, $N = 499$, $\gamma_0 = 30$, $\sigma = 2$, $l = 50$, $\eta = 0.05$. For units see Appendix A.

Since (15) complicates further calculations, we expanded it into a series around $\sqrt{\gamma}/(2\pi)$ equal to zero. Expression (14) is taken directly from Lieb and Liniger paper [15] – see Eqs. (3.32) and Appendix A.

To test above approximations we compare the shock wave solutions that neglect the QP term and use approximate expression for $\sqrt{\frac{1}{\rho} \frac{\partial \mu}{\partial \rho}}$, to the full numerical solution of hydrodynamic equations (4,5,6). Initially we determine velocity field from (12) and choose

$$\rho(x, 0) = \rho_0 + \frac{\eta \rho_0}{\cosh(x/\sigma)^2}, \quad \eta > 0, \quad (16)$$

with $\sigma \gg \xi(\rho)$ (calculations for $\eta < 0$ can be easily repeated). The background density ρ_0 is found from the normalization condition: $\int_{-l}^l dx \rho(x, 0) = N$, where we have assumed that periodic box has boundaries at $\pm l$. For well localized perturbations being of interest from now on one gets $\rho_0 = \frac{N}{2(l+\eta\sigma)}$. Finally, it is convenient to define relative density

$$\varrho = \frac{\rho}{\rho_0}.$$

Now we consider separately $\gamma > \gamma_c$ and $\gamma < \gamma_c$ cases.

A. $\gamma \geq \gamma_c$ case

The healing length is found from (10) and Eqs. (3.32) of [15] subjected to rescalings of Appendix A

$$\xi(\rho) = \frac{1}{\pi\rho} \left(1 + \frac{8}{3\gamma} + \frac{2}{3\gamma^2} \right), \quad (17)$$

where the first term corresponds to the Fermi length of a non-interacting Fermi gas – a result that may be expected from the FBMT [13].

Rewriting implicit solution (11) to the form

$$\varrho(x, t) = f(x - c_\infty w_\infty(\varrho) t),$$

where $c_\infty = \pi\rho_0$ is a background sound velocity of a Tonks gas, one gets from (11) and (14)

$$w_\infty(\varrho) = \frac{2\varrho + s\varrho^2 - 1}{(1 + s\varrho)^2(1 + s)}, \quad s = \frac{2}{\gamma_0}.$$

Taking (16) as an initial density profile, the implicit shock-wave solution reads:

$$\varrho(x, t) = 1 + \frac{\eta}{\cosh[(x - c_\infty w_\infty(\varrho)t)/\sigma]^2}. \quad (18)$$

Although, the explicit form of $\varrho(x, t)$ can not be extracted analytically, important properties of pulse dynamics can be determined. First of all, impulse amplitude, $1 + \eta$, is constant in time. Second, speed of impulse maximum for any $\eta > 0$ equals

$$\mathcal{V}(\eta) = c_\infty w_\infty(1 + \eta),$$

and applicability of this expression is not limited to $1/\cosh(x/\sigma)^2$ perturbations only – Sec. IV. Third, the width of the impulse at given density is constant during propagation – a property that we missed in earlier papers [5, 10]. Fourth, impulse tails propagate roughly with the background sound velocity equal to $c_\infty w_\infty(1)$, while the impulse maximum moves with the speed $c_\infty w_\infty(1 + \eta)$. Since $w(\varrho)$ monotonically increases with ϱ , the impulse deforms its shape so that a shock wave front forms, i. e., $|\partial_x \rho(x, t)| = +\infty$ at one point.

Time and position of shock-wave creation can be extracted from equations [24]:

$$\partial_\rho x(\rho) = 0, \quad \partial_\rho^2 x(\rho) = 0. \quad (19)$$

Their solution gives: density ρ_s at which density profile becomes locally vertical, and time t_s at which this occurs:

$$\varrho_s = \frac{3 + 4s\eta + 9s - \sqrt{9(1+s)^2 + 16s^2\eta^2}}{6s}, \quad (20)$$

$$t_s = \frac{\sigma\sqrt{\eta}}{4c_\infty(\varrho_s - 1)\sqrt{1 + \eta - \varrho_s}}. \quad (21)$$

These expressions close to a Tonks gas limit take a simple form:

$$\rho_s = 1 + \frac{2}{3}\eta + \mathcal{O}\left(\frac{1}{\gamma}\right), \quad t_s = \frac{3\sqrt{3}}{8} \frac{\sigma}{\eta c_\infty} + \mathcal{O}\left(\frac{1}{\gamma}\right).$$

Comparison of analytical solution (18) and full numerical one based on hydrodynamic equations (4,5,6) is presented in Fig. 2. As easily seen, there is a good agreement

between hydrodynamical solution and a shock-wave one until the moment of shock creation. Then discrepancy increases due to appearance of density oscillations triggered by the QP term (7) neglected in derivation of (18). Since presence of the QP term for large γ , e.g., $\gamma \geq \gamma_c$, is questionable, it is an interesting open question whether density oscillations in the form presented in Fig. 2 survive or not for any $\gamma \geq \gamma_c$ considered here.

B. $\gamma < \gamma_c$ case

The healing length reads

$$\xi(\rho) = \frac{1}{\sqrt{2a\rho}} \left(1 + \frac{\sqrt{\gamma}}{2\pi} + \frac{3\gamma}{8\pi^2} \right), \quad (22)$$

derived by extraction of $\mu(\rho)$ from (15) and subsequent Taylor expansion of (10). Naturally, the first term in (22) corresponds to the BEC healing length.

The implicit shock-wave solution has the form:

$$\varrho(x, t) = f(x - c_0 w_0(\varrho)t), \quad (23)$$

where $c_0 = \sqrt{a\rho_0}$ is the background speed of sound in the limit of $\gamma \rightarrow 0$. Combining (11) and (13) one gets

$$w_0(\varrho) = 3\sqrt{\varrho} - 2 - \frac{\sqrt{\gamma_0}}{4\pi} (\ln \varrho + 1) + \frac{\gamma_0}{32\pi^2} \left(\sqrt{\frac{1}{\varrho}} - 2 \right) - \frac{\gamma_0^{3/2}}{128\pi^3}. \quad (24)$$

To verify accuracy of (23) we have simulated dynamics for the system with $\gamma_0 = a/\rho_0 = 5$, i. e., for γ_0 outside the BEC mean-field regime (see inset of Fig. 1), but small enough to stay clearly within $\gamma < \gamma_c$ parameter range. Agreement between full numerical solution of Eqs. (4,5) and implicit shock solution is good before shock formation. Close to time of shock creation discrepancies show up in the oscillatory region missed in (23). Qualitatively, the plot that presents these results is the same as Fig. 2.

Since dynamics of initial density profile is qualitatively the same as in the $\gamma \geq \gamma_c$ case, we notice that impulse maximum moves now for any $\eta > 0$ with velocity

$$\mathcal{V}(\eta) = c_0 w_0(1 + \eta).$$

The explicit solution of shock equations (19) can be found in the limit of $\gamma_0 \rightarrow 0$, but still arbitrary $\eta > 0$:

$$\rho_s = \frac{1 + \eta + \sqrt{(1 + \eta)(9 + \eta)}}{4},$$

$$t_s = \frac{\sigma \sqrt{\eta \rho_s}}{3c_0(\rho_s - 1)\sqrt{1 + \eta - \rho_s}}.$$

Interestingly, for a gaussian like initial impulse discussed in [5] explicit expressions for ρ_s and t_s in this limit were beyond the reach. Finally, we note that the QP term for $\gamma \rightarrow 0$ is certainly present, but it is hard to say whether it survives in (5) for any $\gamma < \gamma_c$. Since the QP term affects shock dynamics strongly, an experiment should clarify this uncertainty.

IV. PROPAGATION OF PULSES OF ARBITRARY SHAPE

In this section we describe some general properties of shock-wave solutions (11,12). To this aim we consider density profiles satisfying

$$\rho(x, t) = f(x - W(\rho)t) = f(\zeta). \quad (25)$$

Suppose that there are n extrema (minima, maxima), placed on a background density ρ_0 , in the initial density profile $\rho(x, 0)$. Let us denote positions of these extrema at $t = 0$ as $x_i(0)$ and set $\rho_i = \rho(x_i(0), 0)$. It means that $\partial_x f(x)|_{x_i(0)} = 0$ and $\partial_x^2 f(x)|_{x_i(0)} \neq 0$. At $t > 0$ one gets from (25)

$$\partial_x \rho(x, t) = \frac{\frac{\partial f(\zeta)}{\partial \zeta}}{1 + \partial_\rho W(\rho) \frac{\partial f(\zeta)}{\partial \zeta} t},$$

which obviously equals zero iff $\zeta = x_i(0)$. It implies that $x_i(t) = x_i(0) + W(\rho_i)t$. Furthermore, we have $\partial_x^2 \rho(x, t)|_{x_i(t)} = \partial_x^2 \rho(x, 0)|_{x_i(0)} \neq 0$, which proves that extrema do not change into saddle points in the course of time evolution. This means that velocity of impulse extrema equals $W(\rho_i)$, where $\rho_i = \rho(x_i(t), t) = \rho(x_i(0), 0)$.

Since $W(\rho)$ is shape independent, we conclude that for any γ density extrema propagate with constant amplitude and speed equal to $W(\rho_i)$. This speed is well approximated as

$$0 < \gamma < \gamma_c : \quad c_0 w_0(\rho_i/\rho_0), \quad (26)$$

$$\gamma > \gamma_c : \quad c_\infty w_\infty(\rho_i/\rho_0), \quad (27)$$

for γ 's a little off γ_c .

Finally, it is important to stress that above statements concerning the amplitude and velocity of density extrema are valid at least as long as the implicit solution works, i. e., up to the time of shock creation. After that time, they are valid in regions far enough from shock structures.

V. EXPERIMENTAL REALIZATION

As discussed in [5, 10], experimental creation of matter-wave packets undergoing shock-wave dynamics is straightforward. The idea is to cool atoms in an additional external potential created by a well-detuned laser beam, and then suddenly turn the beam off. The term suddenly, means on time scale much smaller than time of sound propagation through the perturbation.

The initial density of atoms resulting from an external laser potential V_l is determined as follows. Combining density ρ and velocity field $v = \partial_x \chi$ into $\phi = \sqrt{\rho} \exp(i\chi)$ the Eqs. (4,5) can be rewritten to the standard form

$$i\partial_t \phi = -\frac{1}{2} \partial_x^2 \phi + V_l(x) \phi + \mu(\rho) \phi, \quad (28)$$

which time-independent version reads

$$-\frac{1}{2}\partial_x^2\phi + V_l(x)\phi + \mu(\rho)\phi = \tilde{\mu}\phi,$$

with $\tilde{\mu}$ being a chemical potential. Assuming that the laser potential induces density changes on length scales larger than the healing length (10), one determines an initial density profile from

$$V_l(x) + \mu(\rho) = \tilde{\mu},$$

with $\tilde{\mu}$ found from $\int dx \rho = N$. Naturally, velocity field equals zero in an initial state considered here.

A straightforward generalization of results from [5, 10] shows that if the initial density profile is $\rho(x, 0) = \rho_0 + h(x)$ with $\max|h(x)| \ll \rho_0$ then $\rho(x, t) = \rho_0 + h(x - v_s(\rho_0)t)/2 + h(x + v_s(\rho_0)t)/2$, with $v_s(\rho_0)$ being background sound velocity (3). Therefore, there are left and right moving perturbations. Due to mirror symmetry, we can forget about the left moving one once the pulses are well separated. The right-moving pulse is described by $\rho_0 + h(x - v_s(\rho_0)t)/2$ as long as $t \ll t_s$, since even arbitrarily small density perturbations experience a shock deformation after long enough evolution.

In BEC and Tonks limits qualitatively the same splitting process takes place even when $\max|h(x)|/\rho_0 \sim 1$ [5, 10]. When the initial density profile is $\rho(x, 0) = \rho_0 + h(x)$, the right moving pulse is described by $\rho(x, t) \approx \rho_0 + f(x - W(\rho)t)$ with $W(\rho)$ being the same as in (25) and $f(x) = h(x)/2$. We checked by solving hydrodynamic equations (4,5) that above described splitting process works qualitatively the same way for any γ , as it works for $\gamma \rightarrow 0, +\infty$ [5, 10]. This observation explains how we imagine practical generation of matter-wave pulses described in previous sections.

VI. APPLICABILITY OF THE GROSS-PITAEVSKII MEAN-FIELD APPROACH TO SHOCK PROBLEMS

In the BEC limit system dynamics in the mean-field approximation (8) is described by the following version of Eq. (28)

$$i\partial_t\phi = -\frac{1}{2}\partial_x^2\phi + V_l(x)\phi + aN|\phi|^2\phi \equiv H_{GP}\phi, \quad (29)$$

where $\int dx |\phi(x, t)|^2 = 1$. This is the Gross-Pitaevskii (GP) equation, which can be rigorously derived by different means – see, e.g., [18, 25].

To go beyond the mean-field approximation we employ a second quantization formalism, i. e., we transform Hamiltonian (1) with an additional potential term, $V_l(x)$, into the form

$$\hat{H} = \int dx \hat{\Psi}^\dagger \left(-\frac{1}{2}\frac{\partial^2}{\partial x^2} + V_l(x) + \frac{a}{2}\hat{\Psi}^\dagger\hat{\Psi} \right) \hat{\Psi}, \quad (30)$$

where $\hat{\Psi}$ is a field operator. In the number conserving Bogolubov approach [25] it reads

$$\hat{\Psi} = \hat{a}_0\phi + \delta\hat{\Psi},$$

with \hat{a}_0 annihilating a particle from a condensate, and $\delta\hat{\Psi}$ annihilating a particle from modes orthogonal to the condensate one. Naturally, ϕ is a condensate mode, i. e., it is an eigenstate of a single particle density matrix, $\langle \hat{\Psi}^\dagger(x')\hat{\Psi}(x) \rangle$, to the highest eigenvalue ($\lambda_0 \sim N$):

$$\int dx' \langle \hat{\Psi}^\dagger(x')\hat{\Psi}(x) \rangle \phi(x') = \lambda_0\phi(x).$$

The single particle density of atoms, $\langle \hat{\Psi}^\dagger(x)\hat{\Psi}(x) \rangle$, equals

$$\langle \hat{a}_0^\dagger\hat{a}_0 \rangle |\phi(x)|^2 + \sum_k |v_k(x)|^2, \quad (31)$$

where the first term accounts for condensate density while the second one corresponds to density of depleted atoms. In further calculations we need both u_k and v_k , e. g., for finite temperature calculations. Indeed, density of atoms at sufficiently low temperature T ($\lambda_0(T)/N \sim 1$) equals [25]

$$\langle \hat{a}_0^\dagger\hat{a}_0 \rangle |\phi(x)|^2 + \sum_k \langle \hat{b}_k^\dagger\hat{b}_k \rangle \langle u_k|u_k \rangle + \sum_k \langle \hat{b}_k^\dagger\hat{b}_k + 1 \rangle \langle v_k|v_k \rangle, \quad (32)$$

where $\langle \hat{b}_k^\dagger\hat{b}_k \rangle = [\exp(\omega_k/(k_B T)) - 1]^{-1}$. To get u_k , v_k and ω_k one first finds a condensate mode from the time-independent GP equation, $H_{GP}\phi = \tilde{\mu}\phi$, and then constructs the matrix

$$\mathcal{L} = \begin{pmatrix} H_{GP} + aNQ|\phi|^2 - \tilde{\mu} & aNQQ\phi^2 \\ -aNQ^*\phi^{*2} & -H_{GP} - aNQ^*|\phi|^2 + \tilde{\mu} \end{pmatrix},$$

where Q is a projector to space orthogonal to a condensate mode: $Q\psi = \psi - \phi\langle\psi|\phi\rangle$. The modes and frequencies are found from the eigen equation

$$\mathcal{L} \begin{pmatrix} u_k \\ v_k \end{pmatrix} = \omega_m \begin{pmatrix} u_k \\ v_k \end{pmatrix},$$

while their dynamics is captured by

$$i\frac{\partial}{\partial t} \begin{pmatrix} u_k \\ v_k \end{pmatrix} = \mathcal{L} \begin{pmatrix} u_k \\ v_k \end{pmatrix},$$

where $\tilde{\mu}$ is set to zero in \mathcal{L} , and the calculation of operator \mathcal{L} at every time step requires simultaneous solution of the time-dependent Gross-Pitaevskii equation. Expressions for densities of atoms (31) and (32) are unchanged in a time dependent case. For a list of u , v modes properties, and details of the number-conserving Bogolubov approach see [25].

It is important to realize what are limitations of the Bogolubov approach. To simplify notation we discuss $T = 0$ case now (the results for $T \neq 0$ can be easily obtained). The Bogolubov method fails in the following two

situations. First, the global breakdown, shows up when total number of depleted atoms, i. e., $\int dx \sum_k |v_k(x)|^2$, becomes comparable to number of atoms in the system. This limitation comes directly from derivation of Bogolubov Hamiltonian [25]. Second, local breakdown, happens when density of depleted atoms becomes comparable to condensate density on a length scale of the order of the healing length:

$$\int_{x-f\xi}^{x+f\xi} dx' N |\phi(x')|^2 \sim \int_{x-f\xi}^{x+f\xi} dx' \sum_k |v_k(x')|^2, \quad (33)$$

with $f = \mathcal{O}(1)$. To clarify (33), we notice that in the Bogolubov approach an impact of noncondensed atoms on condensed ones is neglected. Indeed, to get Bogolubov dynamics one solves a time-dependent GP equation and then puts this solution into equations of motion of noncondensed atoms. In this way noncondensed particles are influenced by condensed ones but not other way round. Next order corrections take into account change of condensate density as a result of repulsive interactions between condensed and noncondensed clouds, and lead to modifications of the GP equation. The correction to the right hand side of (29) is qualitatively of the form $V_{\text{depl}}\phi$ (Eqs. (95,96) in [25]), where

$$V_{\text{depl}}(x) \cong 2a \sum_k |v_k(x)|^2, \quad (34)$$

so that $V_{\text{depl}}(x)$ can be regarded as an external potential acting on a condensate. Extension of changes of condensate density induced by an external, localized potential, is given by the healing length [18]. Therefore, impact of depleted atoms on a condensate is best given by comparison of the new term, V_{depl} averaged over a few healing lengths, to previously dominating term in the GP equation, $aN|\phi(x)|^2$, averaged on the same set of points. It gives the condition (33). Appearance of such a local breakdown of Bogolubov approach will be shown after breaking of a dark shock density profile resulting in soliton production.

Finally, let us comment when condensate depletion might affect mean-field predictions. Since density of depleted atoms depends on the product of a and N only, it is unaffected by the limit

$$N \rightarrow +\infty, \quad a \rightarrow 0, \quad aN = \text{fixed},$$

while the condensed part in total atomic density grows as $\langle \hat{a}_0^\dagger \hat{a}_0 \rangle \sim N$ (31,32). It means that in this limit, being to some extent possible with the help of Feshbach resonances [26], density of depleted atoms does not affect density measurements. The exception might happen when there is dynamical instability leading to fast increase of depleted fraction. Then sooner or later density of depleted atoms will start to have an important impact on condensate dynamics.

In a generic experimental situation, however, a fraction of depleted atoms is non-negligible. To compare a

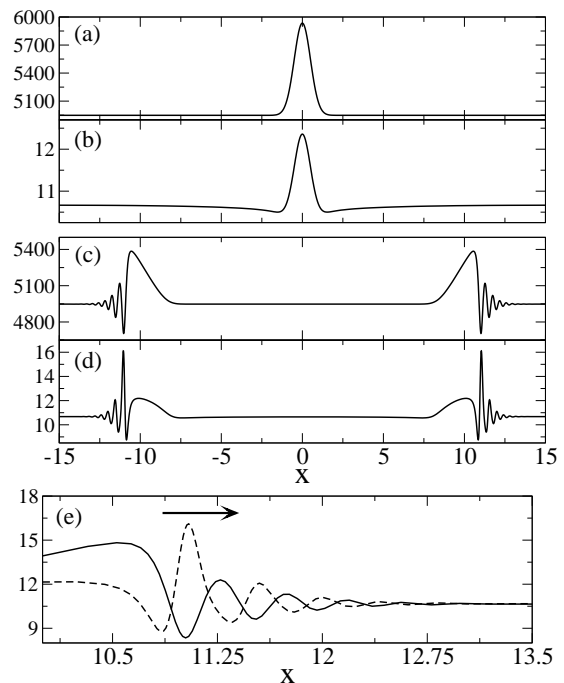


FIG. 3: Density of a condensate, $\langle \hat{a}_0^\dagger \hat{a}_0 \rangle |\phi(x)|^2$, at $t = 0, 0.6$: (a) and (c). Density of depleted atoms ($\sum_{k=0}^{317} |v_k(x)|^2$) at $t = 0, 0.6$: (b) and (d). Plot (e): comparison between condensate density (solid line) and density of depleted atoms (dashed line) in the right-moving shock structure; condensate density is rescaled for presentational purposes. At $t = 0$ laser potential V_l was $\propto -\exp(-2x^2)$ and the system was in a ground state; $V_l(t > 0) \equiv 0$. The number of noncondensed atoms equals ~ 320 during whole evolution. Total number of atoms is $1.5 \cdot 10^5$. Other parameters: $l = 15$, $aN = 7500$, $T = 0$. Time of shock creation obtained from [5] is $t_s = 0.36$. For units see Appendix B.

mean-field prediction to quantum many-body dynamics, we have chosen a particular set of experimentally accessible parameters – see Appendix B for details.

In the following we discuss evolution of shock structures resulting from white ($\eta > 0$) and dark ($\eta < 0$) initial density profiles, where η stands for relative perturbation amplitude: as in Eq. (16). Since corrections to mean field equations are very different in these two cases we discuss them separately.

White shock waves: We have done different calculations changing not only the size of an initial perturbation but also aN , N , etc. In all cases we observe that total depletion of a condensate negligibly increases from beginning of time evolution to appearance of well developed shock structures. Density of depleted atoms around shocks becomes at most $\mathcal{O}(1)$ larger than depletion density far away from perturbations. Therefore, if density and distribution of depleted atoms was such that the Bogolubov approach was initially applicable, it will also work during shock creation and propagation.

The results for experimentally relevant choice of parameters are depicted in Fig. 3. As easily seen from

differences in scales between Figs. 3(a), (c) and Figs. 3(b), (d), the corrections to the mean-field result are minor. Repulsion between condensed and depleted atoms, results in localization of depleted atoms around condensate density minima: Fig. 3(e). This was predicted by us in [5], however, the amount of depleted atoms, turns out to be insufficient to fill condensate ripples.

We have also done finite temperature calculations according to (32). At $T \neq 0$ not only quantum depletion but also thermal one shows up, which leads to increase of total number of depleted atoms in comparison to the $T = 0$ situation. We have considered low temperatures, i. e., $T \leq 30\text{nK}$ (see Appendix B), to see whether thermal effects qualitatively affect shock dynamics. The only difference with respect to $T = 0$ case is that total depletion is larger by a factor of $\mathcal{O}(10)$ for $T \sim 30\text{nK}$, which is still not enough for getting significant corrections to BEC shocks from depleted atoms.

These calculations suggest that the Gross-Pitaevskii equation captures correctly physics of white shock waves in a BEC. Finite temperature effects does not seem to destroy the qualitative picture of shock formation and propagation given by the mean-field approach.

Dark shock waves: Dark density profiles undergo two distinct stages of evolution. In the first one, shock waves form, while in the second one shock density profile breaks into a train of solitons that move, according to the mean-field approach, with constant velocity and without changes of shape. The same was independently observed numerically in [27] and theoretically in [28]. Theoretical predictions in both papers are based solely on the basis of mean-field equations.

As in white shocks calculations, we have fixed the parameters to those experimentally relevant—see Appendix B. The formation of shock wave structures is depicted in Figs. 4(a), (b), (c), (d). Now a rear impulse edge self-steepens instead of a front one. This comes from the fact that now impulse tail moves faster than impulse center, i. e., density minimum. In the case considered in Fig. 4, a shock profile breaks before complete separation. Obviously, if the impulse would be more shallow the breakdown would happen later. As easily seen, the correction to total density coming from depleted atoms can be neglected at this stage of time evolution.

After shock breakdown, solitons are produced as depicted in Fig. 4(e). Then density of depleted atoms increases by orders of magnitude. It results in significant corrections to total density of atoms and causes local, i. e., around soliton minima, breakdown of the Bogolubov approach according to (33). Notice that still fraction of depleted atoms, less than 0.7% in Fig. 4(f), is so small that the global condition of Bogolubov approach applicability is well satisfied. As depicted in Fig. 5 both peak density of depleted atoms at soliton minimum (dots) and total depletion of a condensate (squares) follow approximately power law increase from the moment of soliton train formation.

It is easy to predict qualitatively what are correc-

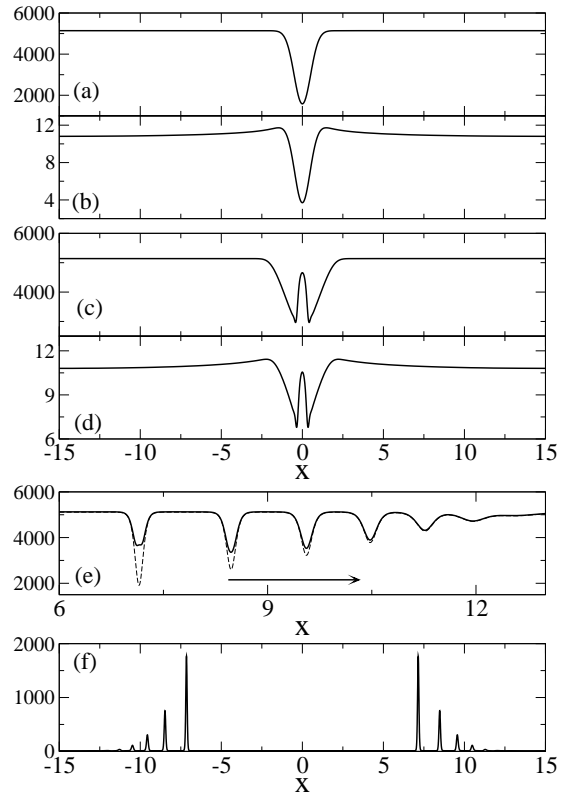


FIG. 4: Density of a condensate, $\langle \hat{a}_0^\dagger \hat{a}_0 \rangle |\phi(x)|^2$, at $t = 0, 0.06$: (a) and (c). Density of depleted atoms ($\sum_{k=0}^{349} |v_k(x)|^2$) at $t = 0, 0.06$: (b) and (d). Plot (e): black thick line – total density of atoms, dashed line – condensate density; both curves are for right-moving dark-shock-originated soliton train at $t = 0.75$. Plot (f): density of depleted atoms at $t = 0.75$. External laser potential at $t = 0$ was $\propto \exp(-2x^2)$ and the system was in a ground state; $V_i(t > 0) \equiv 0$. The number of noncondensed atoms equals ~ 320 at $t = 0$ and ~ 1000 at $t = 0.75$. The total number of atoms equals $1.5 \cdot 10^5$. Other parameters: $l = 15$, $aN = 7500$, $T = 0$. Time of shock creation obtained from [5] is $t_s = 0.086$. For units see Appendix B.

tions to a Bogolubov result coming from depleted atoms. The next order corrections to the Bogolubov approach come from inclusion of repulsive interactions between condensed and non-condensed atoms. It is qualitatively accounted for by introducing a new potential term, Eq. (34), into the Gross-Pitaevskii equation. It means that soliton structures in condensate density will become wider, so that depleted atoms will have more space to distribute themselves inside solitons. Therefore, increase of peak density of depleted atoms will certainly slow down. This observation is supported by nonperturbative calculation of Dziarmaga [29], who found that total density of atoms at soliton minimum approaches background density for large times.

Such a fast increase in density of depleted atoms around soliton minima is rather a generic phenomenon. Indeed, it was first theoretically discussed for phase-imprinted solitons in harmonic traps [30, 31] as a mech-

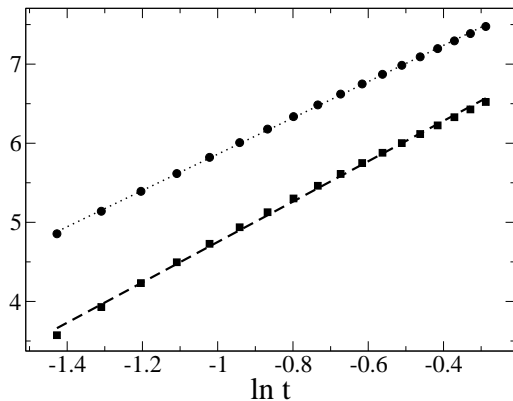


FIG. 5: Introducing notation: p - peak density of depleted atoms in the deepest soliton moving to the right (Fig. 4e); dN - total number of depleted atoms. Dots: $\ln p(t)$; dotted line: a linear fit to circles, with slope given by 2.29. Squares: $\ln[dN(t) - dN(0)]$; dashed line: linear fit with slope equal to 2.55. The data is plotted from $t = 0.24$, i.e., a moment of the deepest soliton creation. For the parameters: see Fig. 4, while for units see Appendix B.

anism for fast disappearance of solitons in the Hannover experiment [32]. The experimental time scale for soliton disappearance was found both theoretically [29, 31] and experimentally [32] to be $\mathcal{O}(10\text{ms})$. Our calculation, based on the same value of nonlinear parameter $aN = 7500$, gives the same estimation for instant when corrections to dynamics of dark-shock-originated solitons become important. Indeed, the time instant 0.75 in Fig. 4(e), corresponds to $\sim 12\text{ms}$ — see Appendix B for a unit of time.

To end this section we recall that predictions presented here apply to a 1D BEC system. There was recently an attempt to experimentally verify applicability of the mean-field approach to shock phenomena [33]. The conclusion was that the ripples in a white shock wave front are not filled with depleted atoms. Our present work supports this observation assuming that 1D results are qualitatively correct in 2D rapidly rotating array of vortices on top of which a white shock wave front propagates.

VII. SUMMARY

This paper presents a complete hydrodynamical description of basic properties of shock-waves in a delta interacting 1D Bose gas. Our predictions can be directly verified experimentally. In principle, a proper experimental setup should answer at what Lieb-Liniger parameter γ the quantum pressure term starts to lead to unphysical results. Notice that density oscillations in front of a shock wave are present due to this term for small enough γ , while for large γ they are absent in exact solution and shocks propagate in a very different way [10]. In fact, a change of this kind in shock dynamics can be a nice experimental signature of a BEC-Tonks crossover.

We also discussed quantum many-body corrections to Gross-Pitaevskii shock-wave solutions. This way we clarified the role of depleted atoms in shock dynamics. This important point was missed in previous studies of BEC shock waves [5, 6, 7, 8, 9].

From experimental point of view, tools for verification of our predictions seem to be available either right now or in the nearest future. Indeed, a first experiment on sound propagation in a BEC was done years ago [34]. Since we do not discuss time-of-flight measurements the best comparison between our theory and experiment should rely on *in situ* measurements [34]. The most prospective experimental setup for observation of shock dynamics in different γ parameter ranges is probably provided by a box-like optical trap [4], where values of $\gamma \leq 1$ approaching the BEC-Tonks crossover (Fig. 1), have been already achieved. Other interesting experimental setups include atom chips [35] and circular atom waveguides [11]. The latter one, being best suited for studies of shock collisions.

From theoretical side, there are at least two possible interesting extensions of this work. First of all, one can analyze shock dynamics in quasi-1D trapping geometries, where the system is a 3D waveguide with adjustable harmonic transverse confinement. This can be easily done using results from [36]. Indeed, instead of Eq. (6) one can consider Eq. (5) of [36] and repeat subsequent calculations. In the limit of tight transversal confinement, i. e., for a 1D Bose gas, both expressions for $\mu(\rho)$ lead to physically identical results. The second interesting extension of this work includes studies of possible outcomes of a single shot density measurement. In fact, it should be stressed that predictions based on hydrodynamical and Bogolubov approaches apply to averages over different experimental measurements done on the system prepared many times in the same quantum state. Needless to say, averages may differ from a single shot outcomes— see [37] for an illustrative example.

I would like to acknowledge discussions with Zbyszek Karkuszewski. This work was started in the Institute for Theoretical Physics in Hannover. I'm grateful to both the Alexander von Humboldt Foundation for support of this work in Germany, and to the US Department of Energy for support of this research at the LANL.

APPENDIX A: UNITS IN A BOX

Since this paper uses extensively results of [14, 15] it is useful to link dimensionless quantities used by us to those of [14, 15].

The eigen equation of a 1D Hamiltonian expressed in terms of dimensional quantities denoted by primes is

$$-\frac{\hbar^2}{2m} \sum_i \frac{\partial^2}{\partial x_i'^2} \Psi + A' \sum_{i < j} \delta(x_i' - x_j') \Psi = E' \Psi, \quad (\text{A1})$$

to get dimensionless Hamiltonian (1) one introduces: $x_i' = x_i l_0$, $E' = E \hbar^2 / (m l_0^2)$, $A' = a \hbar^2 / (m l_0)$, where l_0

is an arbitrary length scale. Consideration of a time-dependent Schrödinger equation leads to $t' = t m l_0^2 / \hbar$.

The dimensionless Hamiltonian used by Lieb and Liniger has the form

$$\hat{H} = - \sum_i \frac{\partial^2}{\partial x_i^2} + 2c \sum_{i < j} \delta(x_i - x_j),$$

and can be obtained from (A1) after rescalings: $x'_i = x_i l_0$, $E' = E \hbar^2 / (2m l_0^2)$, $A' = c \hbar^2 / (m l_0)$, $t' = t 2m l_0^2 / \hbar$.

Therefore, there are the following relations between our dimensionless quantities and Lieb and Liniger ones marked by LL:

$$\gamma = \gamma_{LL} \quad , \quad \mu = \frac{\mu_{LL}}{2} \quad , \quad v = \frac{v_{LL}}{2},$$

where v is sound velocity. Finally we note, that there is a misprint in the first line of expression (1.4) providing sound velocity [14]. There should be $-2\gamma de/d\gamma$ (as used in Sec. II) instead of $-\gamma de/d\gamma$. The second line of (1.4) in [14] is correct.

APPENDIX B: A BOX APPROXIMATION OF A 3D SYSTEM IN THE BEC LIMIT

We aim at getting a 1D box approximation of a full 3D BEC gas confined in a 3D harmonic potential. The system in the mean-field approximation satisfies the following 3D Gross-Pitaevskii equation

$$i\hbar \frac{\partial \Psi'}{\partial t'} = - \frac{\hbar^2}{2m} \vec{\nabla}'^2 \Psi' + (m\omega^2 x'^2/2 + m\omega_\perp^2 r'^2/2) \Psi' + g'_{3D} |\Psi'|^2 \Psi',$$

where $\omega_\perp \gg \omega$, $g'_{3D} = 4\pi \hbar^2 a_{sc} N / m$ with a_{sc} being interatomic scattering length, and $\int d^3 x' |\Psi'|^2 = 1$. First, we rescale all quantities using the harmonic oscillator units in the x' direction. Denoting by symbols without primes dimensionless quantities,

$$(x', y', z') = (x, y, z) \sqrt{\frac{\hbar}{m\omega}}, \quad \Psi' = \Psi \left(\frac{m\omega}{\hbar} \right)^{3/4}, \quad t' = \frac{t}{\omega},$$

we arrive at the following 3D GP equation

$$i \frac{\partial \Psi}{\partial t} = - \frac{1}{2} \vec{\nabla}^2 \Psi + (x^2/2 + \lambda^2 r^2/2) \Psi + g_{3D} |\Psi|^2 \Psi,$$

where λ is trap aspect ratio ω_\perp/ω while $g_{3D} = 4\pi a_{sc} N \sqrt{m\omega/\hbar}$. This equation can be derived from the following energy functional:

$$\mathcal{E}[\Psi] = \int d^3 x \left[\frac{1}{2} |\vec{\nabla} \Psi|^2 + (x^2/2 + \lambda^2 r^2/2) |\Psi|^2 + \frac{g_{3D}}{2} |\Psi|^4 \right]. \quad (\text{B1})$$

To proceed further we assume a simple form of a variational wave-function,

$$\Psi(x, r) = \phi(x) \exp \left(- \frac{r^2}{2l_\perp^2} \right) \frac{1}{\sqrt{\pi} l_\perp}, \quad (\text{B2})$$

where $\int dx |\phi(x)|^2 = 1$ and l_\perp is a variational parameter. Substituting (B2) into (B1) one gets

$$\mathcal{E}[\phi] = \int dx \left[\frac{1}{2} |\partial_x \phi|^2 + \frac{x^2}{2} |\phi|^2 + \frac{g_{3D}}{4\pi l_\perp^2} |\phi|^4 \right] + \frac{l_\perp^2 \lambda^2}{2} + \frac{1}{2l_\perp^2}, \quad (\text{B3})$$

which supports the following 1D GP equation

$$i \partial_t \phi = - \frac{1}{2} \partial_x^2 \phi + \frac{x^2}{2} \phi + aN |\phi|^2 \phi, \quad (\text{B4})$$

with $aN = g_{3D}/(2\pi l_\perp^2)$. To determine l_\perp , we substitute the Thomas-Fermi solution of (B4),

$$aN |\phi(x)|^2 = \frac{1}{2} \left(\frac{3aN}{2} \right)^{2/3} - \frac{x^2}{2}, \quad (\text{B5})$$

into (B3) getting $\mathcal{E}(l_\perp)$, which minimization leads to

$$(g_{3D} l_\perp)^{2/3} = (250\pi^2/9)^{1/3} (\lambda^2 l_\perp^4 - 1).$$

In the limit of $g_{3D} \rightarrow 0$ one gets $l_\perp = 1/\sqrt{\lambda}$, which is a noninteracting cloud width. In a typical experiment, a cloud width is much larger than $1/\sqrt{\lambda}$ [18], so

$$l_\perp \approx \left(\frac{9}{250\pi^2} \right)^{1/10} \frac{g_{3D}^{1/5}}{\lambda^{3/5}}.$$

For a cigar shaped cloud one can assume, e.g., $\omega = 2\pi \cdot 10\text{Hz}$, $\omega_\perp = 2\pi \cdot 569\text{Hz}$. Taking also $N = 1.5 \cdot 10^5$, $a_{sc} = 5.2 \cdot 10^{-9}\text{m}$ (scattering length of ^{87}Rb in the $|F=2, m_F=2\rangle$ state), $m = 89.91 \times 1.66 \cdot 10^{-27}\text{kg}$ (atomic mass of ^{87}Rb), one can find that the units of length and time are $\sim 3.4\mu\text{m}$ and $\sim 16\text{ms}$, respectively. For these parameters $aN \approx 7500$ and the unit of temperature, $\hbar\omega/k_B$, equals 0.48nK . By using all these results it is easy to transform dimensionless plots from Sec. VI, into dimensional ones.

A box approximation of dimensionally reduced harmonically trapped cloud described above is the following. We place exactly the same number of atoms in the box as in the quasi-1D configuration described by (B5). We assume that, in the absence of external laser potential, density in a box extending from $[-l, l]$ is exactly the same as at a center of a harmonic trap: $[3/(4\sqrt{2})]^{2/3}/(aN)^{1/3} = 1/(2l)$, which gives $l = (aN)^{1/3} (2/3)^{2/3}$.

For parameters defined above $2 \cdot l \approx 30$ (about 0.1mm), which can be compared to the Thomas-Fermi size of the harmonically trapped cloud equal here to ~ 44 (about 0.15mm). The box-like approximation leads to results being in good qualitative agreement with calculations done in a harmonically trapped case. It concerns both length and time scales of shock dynamics.

-
- [1] V.E. Korepin, N.M. Bogoliubov and A.G. Izergin, *Quantum inverse scattering method and correlation functions*, (Cambridge University Press, Cambridge, 1993).
 - [2] H. Moritz, T. Stöferle, M. Köhl and T. Esslinger, Phys. Rev. Lett. **91**, 250402 (2003).
 - [3] B. Paredes, A. Widera, V. Murg, O. Mandel, S. Fölling, I. Cirac, G.V. Shlyapnikov, T.W. Hansch and I. Bloch, Nature **429**, 277 (2004).
 - [4] T.P. Meyrath, F. Schreck, J.L. Hanssen, C.-S. Chuu and M.G. Raizen, Phys. Rev. A **71**, 041604(R) (2005).
 - [5] B. Damski, Phys. Rev. A **69**, 043610 (2004).
 - [6] A.M. Kamchatnov, A. Gammal and R.A. Kraenkel, Phys. Rev. A **69**, 063605 (2004).
 - [7] V.M. Pérez-García, V. V. Konotop and V. A. Brazhnyi, Phys. Rev. Lett. **92**, 220403 (2004).
 - [8] C. Menotti, M. Kraemer, A. Smerzi, L. Pitaevskii and S. Stringari, Phys. Rev. A **70**, 023609 (2004).
 - [9] G.A. El and A.M. Kamchatnov, Phys. Lett. A **350**, 192 (2006).
 - [10] B. Damski, J. Phys. B **37**, L85 (2004).
 - [11] S. Gupta, K.W. Murch, K.L. Moore, T.P. Purdy and D.M. Stamper-Kurn, Phys. Rev. Lett. **95**, 143201 (2005).
 - [12] M. Olshanii, Phys. Rev. Lett. **81**, 938 (1998).
 - [13] M.D. Girardeau and E.M. Wright, Laser Phys. **12**, 8 (2002).
 - [14] E.H. Lieb, Phys. Rev. **130**, 1616 (1963).
 - [15] E.H. Lieb and W. Liniger, Phys. Rev. **130**, 1605 (1963).
 - [16] V. Dunjko, V. Lorent and M. Olshanii, Phys. Rev. Lett. **86**, 5413 (2001).
 - [17] Y.E. Kim and A.L. Zubarev, Phys. Rev. A **67**, 015602 (2003).
 - [18] F. Dalfovo, S. Giorgini, L.P. Pitaevskii and S. Stringari, Rev. Mod. Phys. **71**, 463 (1999).
 - [19] E.B. Kolomeisky and J.P. Straley, Phys. Rev. B **46**, 11749 (1992).
 - [20] E.B. Kolomeisky, T.J. Newman, J.P. Straley and X. Qi, Phys. Rev. Lett. **85**, 1146 (2000); *ibid* **86**, 4709 (2001).
 - [21] D.J. Frantzeskakis, N.P. Proukakis, and P.G. Kevrekidis, Phys. Rev. A **70**, 015601 (2004).
 - [22] A. Minguzzi, P. Vignolo, M.L. Chiofalo, and M.P. Tosi, Phys. Rev. A **64**, 033605 (2001).
 - [23] M.D. Girardeau and E.M. Wright, Phys. Rev. Lett. **84**, 5239 (2000).
 - [24] L.D. Landau and E.M. Lifshitz, *Fluid Mechanics* (Pergamon, Oxford, 1989)– see Sec. 101 for details.
 - [25] Y. Castin and R. Dum, Phys. Rev. A **57**, 3008 (1998).
 - [26] S.L. Cornish, N.R. Claussen, J.L. Roberts, E.A. Cornell and C.E. Wieman, Phys. Rev. Lett. **85**, 1795 (2000).
 - [27] Z. Dutton, M. Budde, C. Slowe and L.V. Hau, Science **293**, 663 (2001).
 - [28] A.M. Kamchatnov, R.A. Kraenkel and B.A. Umarov, Phys. Rev. E **66**, 036609 (2002).
 - [29] J. Dziarmaga, Phys. Rev. A **70**, 063616 (2004).
 - [30] J. Dziarmaga, Z. P. Karkuszewski and K. Sacha, Phys. Rev. A **66**, 043615 (2002).
 - [31] J. Dziarmaga and K. Sacha, Phys. Rev. A **66**, 043620 (2002); C.K. Law, Phys. Rev. A **68**, 015602 (2003).
 - [32] S. Burger, K. Bongs, S. Dettmer, W. Ertmer, K. Sengstock, A. Sanpera, G.V. Shlyapnikov and M. Lewenstein, Phys. Rev. Lett. **83**, 5198 (1999).
 - [33] T.P. Simula, P. Engels, I. Coddington, V. Schweikhard, E.A. Cornell and R.J. Ballagh, Phys. Rev. Lett. **94**, 080404 (2005).
 - [34] M.R. Andrews, D.M. Kurn, H.-J. Miesner, D.S. Durfee, C.G. Townsend, S. Inouye, and W. Ketterle, Phys. Rev. Lett. **79**, 553 (1997); *ibid* **80**, 2967 (1998).
 - [35] A. Kasper, S. Schneider, C. vom Hagen, M. Bartenstein, B. Engeser, T. Schumm, I. Bar-Joseph, R. Folman, L. Feenstra and J. Schmiedmayer, J. Opt. B: Quantum Semiclass. Opt. **5**, S143 (2003).
 - [36] L. Salasnich, A. Parola and L. Reatto, Phys. Rev. A **70**, 013606 (2004).
 - [37] J. Javanainen and S.M. Yoo, Phys. Rev. Lett. **76**, 161 (1996).